

ЖУРНАЛ
ЭКСПЕРИМЕНТАЛЬНОЙ
И ТЕОРЕТИЧЕСКОЙ ФИЗИКИ

ОСНОВАН В МАРТЕ 1873 ГОДА
ВЫХОДИТ 12 РАЗ В ГОД
МОСКВА

ТОМ 111, ВЫПУСК 4
АПРЕЛЬ, 1997
«НАУКА»

COULOMB DISSOCIATION OF INCIDENT ^{16}O AT 4.5 GeV/c

©1997 M. Nabil Yasin, M. M. Sherif, S. M. Abd El-Halim*, M. A. Jilany**

Physics Department Faculty of Science, Cairo University, Giza, Egypt

** Phys. Department Faculty of Science, Banha-Zagazig University, Egypt*

*** Sohag Faculty of Science, South Valley University, Sohag, Egypt*

Submitted 10 April 1996

Projectile multifragment breakup of ^{16}O , ^{12}C and ^7Li at energies 3.0–4.5 A-GeV is studied by means of the Weizsacker–Williams method. The fragmentation channels of the ^{16}O projectile at 4.5 A-GeV are investigated and compared with that of ^{16}O at 200 A-GeV. The events characterized by $N_h = 0$ and these events due to both Coulomb and diffraction dissociation have been selected and analyzed as a function of impact parameter. Also, the dependence of the electromagnetic dissociation cross-section on incident energy and the charge of projectile and target is found.

1. INTRODUCTION

In recent years, nucleus-nucleus collisions at high energies have been attracting more interest as a way to understand the important effects of nuclear interaction mechanisms at different impact parameters b . The reason for the study at small impact parameter is to observe the signatures of unusual forms of nuclear matter such as the quark-gluon plasma [1], while studies at higher values of the impact parameters help in understanding the nuclear structure. Also, the electromagnetic effects [1, 2] which considered as a source of background for these nuclear interactions like the possible features for quark gluon plasma.

Heckman and Greiner [3] reported the first results of a Bevatron experimental on the fragmentation of nitrogen ions by carbon and hydrogen targets at 29 A-GeV.

The point of interest in this work, is the dislocation of fragments from the projectile nucleus. They tried to classify the reactions according to the following categories.

1) Stripping reaction, in which the spectator part of a projectile is diffracted inelastically, while the other part suffers a strong interaction with the target nucleus. These reaction occurs at $R_p + R_t > b > R_p - R_t$, where R_p and R_t are the radii of projectile and target nucleus respectively.

2) More peripheral collision, in which all projectile constituents are dislocated and associated with some hadrons, mostly pions. These interactions occur at large values of the impact parameter b , up to $R_p + R_t$.

3) Pure electromagnetic dissociation of the incident charge nucleus as a result of its passage through the Coulomb field of the target nucleus which provides an electromagnetic pulse of short duration, enhanced due to Lorentz contraction γ . These interactions occur at impact parameters b greater than the sum of the projectile and target nuclear radius (i.e., $b > R_p + R_t$).

2. EXPERIMENT AND RESULTS

2.1. Experimental Details

At the Dubna synchrophasotron BR-2 emulsion stacks were irradiated with beams of 4.5 A-GeV ^{16}O and ^{12}C ions and 3.0 A-GeV ^7Li ions, the dimensions of the pellicells are 20 cm \times 10 cm \times 600 μm . The composition of the emulsion is given in Table 1.

Table 1

Types of nucleus	$^1\text{H}_1$	$^{12}\text{C}_6$	$^{14}\text{N}_7$	$^{16}\text{O}_8$	$^{80}\text{Br}_{35}$	$^{108}\text{Ag}_{47}$
Density (N of atoms/ 10^{22})	3.15	1.412	0.395	0.956	1.028	1.028

Scanning was carried out along the track [4], using two types of binocular microscopes МБИ-9 and Wild, with magnification 10×100 .

A total of 958, 1000, and 968 events were found, giving the interaction mean free paths 12.18 ± 0.33 , 14.4 ± 0.33 and 15.2 ± 0.50 cm for ^{16}O , ^{12}C , and ^7Li respectively.

The charged particles (tracks) produced in each interaction are identified according to the following classes [4].

a) Ionization shower tracks (N_s) with very high velocity $\beta = v/c \geq 0.7$ and relative grain density $g^* = g/g_0 \leq 1.4$, where g_0 is the minimum grain density of the relativistic tracks inside the emulsion. Most of them are mesons, along with some fast hydrogen isotopes.

b) Grey tracks (N_g), which are tracks with range $R \geq 3$ mm and $6 \geq g^* > 1.4$. These are mainly knock-out protons from the target nucleus.

c) Black tracks (N_b), which are slow fragments from the target nucleus with rang $R < 3$ mm and $g^* > 6$.

In emulsion experiments, the term «heavy tracks» is used, and their number is defined as $N_h = N_g + N_b$.

d) The projectile fragments (PF_s) are strongly collimated in the forward hemisphere direction which is determined by the approximation relation:

$$\sin \theta_{PF} \leq \frac{P_f}{P_i},$$

where P_f is the Fermi momentum [5] and P_i is the incident momentum. This gives $\theta_{PF} \leq 3.0^\circ$ at the Dubna energy. Referring to Heckman and other [4-6] the projection angles of the PF_s are measured by finding

$$\operatorname{tg} \theta_{PF} = \frac{\Delta y}{\Delta x},$$

where Δy is the deflection of the measured fragment at a longitudinal distance $\Delta x = 1$ cm from the emission point.

The PF_s with charge $Z \geq 2$ for 708, 1000 and 970 events of ^{16}O , ^{12}C and ^7Li beams respectively were recorded. It is possible to identify the doubly charged fragments ($Z = 2$) by eye. A correct estimation is made by using the δ -ray method [4].

2.2. Selection of Electromagnetic Dissociation Events

Table 2

The ($N_h = 0$) events and the selected one due to both Coulomb and diffraction dissociation in ^{16}O -Em. at 4.5 A-GeV/c and ^{16}O -Em. at 200 A-GeV. The separation of them are deduced from the experimental data

The projectile and energy	^{16}O (4.5 A-GeV/c)		^{16}O (200 A-GeV)	
	No. of events	%	No. events	%
Total analysed events	708	—	920	—
$N_h = 0$ events (peripheral coll. + Coul. & diff. diss. + Simulated ED)	98	13.98 ± 1.4	112	12.00 ± 1.13
ED events (Coulomb diss. + diff. Diss.)	—	—	92	10.00 ± 1.00
Pure ED event (Coulomb diss.)	45	6.35 ± 0.94	—	—
Diff. Diss. on target (associated with pions)	36	5.08 ± 0.85	—	—
The dissociation into α -fragments only	$\begin{matrix} 2 \\ \text{O} \rightarrow 4\alpha \end{matrix}$	0.28 ± 0.19	$\begin{matrix} 3 \\ \text{O} \rightarrow 4\alpha \end{matrix}$	0.30 ± 0.06
Diffraction Diss. into α -fragments	$\begin{matrix} 2 \\ \text{O+Em.} \rightarrow 4\alpha + \text{low energy particle} \end{matrix}$	0.28 ± 0.19	2 in all scanned 2934 events	0.07 ± 0.05
Reference	Present work		[7, 8]	

To distinguish between the nuclear interactions and the Coulomb dissociation events, we must consider the expected characteristics of electromagnetic dissociation (ED) events as described in [7]. Generally these ED events are characterized by $N_h = 0$ events, which means that no slow emitted particles and no lepton pair or β -decay are produced. Also, the incident

Table 3

Fragmentation modes of ^{16}O projectile at 4.5 A- and 200 A-GeV/c

Fragmentation Mode	Fraction of Frag. Chan. of ^{16}O (4.5) A-GeV %	Fraction of Frag. Chan. of ^{16}O (200) A-GeV %
O \rightarrow N + H	42.2 ± 6.2	56.0 ± 4.0
\rightarrow C + 2H	1.8 ± 1.3	14.0 ± 2.0
\rightarrow C + He	5.5 ± 2.2	10.0 ± 2.0
\rightarrow B + He + H	1.8 ± 1.3	3.6 ± 1.0
\rightarrow B + 3H	2.8 ± 1.6	0.8 ± 0.5
\rightarrow Be ...	4.6 ± 2.1	5.5 ± 1.2
\rightarrow Li ...	2.8 ± 1.6	2.5 ± 0.8
\rightarrow 4He	1.8 ± 1.3	0.8 ± 0.5
\rightarrow 3He + 2H	5.5 ± 2.2	4.4 ± 1.1
\rightarrow 2He + 4H	1.8 ± 1.3	3.3 ± 1.0
\rightarrow He + 6H	0.9 ± 0.9	0.8 ± 0.5
Reference	Present Work	[7, 8]

charge (Z_p) must equal to the sum of the produced fragment charges and the emitted angle θ_{fr} should be $\leq 3.0^\circ$ at projectile incident energy 4.5A-GeV.

These stringent selection criteria are applied to the experimental data of ^{16}O interactions at 4.5 A-GeV and compared with that of ^{16}O interactions at 200 A-GeV [7, 8]. It was found that about 6% of the total inelastic interactions are due to the effect of the Coulomb field of the target nucleus on the incident ^{16}O at 4.5 A-GeV, whereas this ratio is about 10% for the same projectile at 200 A-GeV. These results confirm the dependence of the ED cross-section on the incident energy. Table 2 represents the total number of analyzed events for each beam. The ED events can be divided into two categories, one of them is owing to the Coulomb field effect and the other to diffraction on the target surface. This has been corrected for the number of ED events which are not associated with pions as shown in Table 3. Then the angle of the emission fragment ($\theta_{PF} \leq 3.0^\circ$) can be divided into two ranges, the lower range of θ_{PF} ($0-1.5^\circ$) is attributed to the effect of the Coulomb field, and the relatively wider angles up to 3.0° result from the effect of diffraction on the outer surface of the target nucleus.

The given numbers of ED events for ^{16}O at 200 A-GeV are extracted from Refs. [7, 8]. It is clear that these ED events increase with the energy and charge of the incident beam, except for incident ^7Li . This exception may arise because the binding energy of the ^7Li nucleus is smaller than that of the other nuclei, as illustrated in Table 4. The ratio of ^{16}O dislocation into four clusters of α -particles at 4.5 A-GeV is more than twice that of the splitting of ^{16}O (200 A-GeV) into the same number 4α -particles. One reason for this may be the difference in the time the projectile spends inside the Coulomb field of the target nucleus as shown in the last table; this will be discussed in the next section.

Also, the previous conditions could be applied as selection criteria for $N_h = 0$ events of the ^7Li interaction at 3.0 A-GeV in order to determine the two easily identified fragments of $Z = 1$ and $Z = 2$, since the incident projectile has a charge $Z = 3$. These selected events are tabulated in Table 4 and compared with other collected data. The difference in the ED event ratios for incident ^6Li and ^7Li at nearly the same total energy is due to the difference in the

Table 4

The interaction of ${}^6\text{Li}$, ${}^7\text{Li}$, ${}^{12}\text{C}$ and ${}^{16}\text{O}$ at Dubna energies compared with ${}^{16}\text{O}$ at higher energies

Type of projectile and energy (A-GeV)	${}^6\text{Li}$ (4.5)	${}^7\text{Li}$ (3.00)	${}^{12}\text{C}$ (4.5)
Total no. of analysed incl. int.	968	970	1000
$N_h = 0$ events	147	136	98
Fraction %	(15.2 ± 1.25)	(14.02 ± 1.2)	(9.8 ± 1.0)
ED events	70	45	60
Fraction %	(7.2 ± 0.86)	(4.64 ± 0.7)	(6.0 ± 0.77)
Nuclear radius*	2.55 fm	2.42 fm	2.46 fm
Binding energy**	32.09	39.25	92
BE (in MeV)			
BE/N (MeV)	5.35	5.61	7.7
Lorentz factor (γ)	4.51	3.22	4.51
E^{max} (MeV)	99.4	72.0	100.5
Duration time τ_d through Ag target component (sec)	$0.66 \cdot 10^{-18}$	$0.93 \cdot 10^{-18}$	$0.66 \cdot 10^{-18}$
References	[17]	Present work	Present work

Type of projectile and energy (A-GeV)	${}^{16}\text{O}$ (4.5)	${}^{16}\text{O}$ (60)	${}^{16}\text{O}$ (200)
Total no. of analysed incl. int.	708	528	920
$N_h = 0$ events	98	—	112
Fraction %	(13.98 ± 1.4)	—	(12.00 ± 1.13)
ED events	81	31	92
Fraction %	(11.43 ± 1.27)	(5.87 ± 1.05)	(10.00 ± 1.00)
Nuclear radius*	2.73 fm	2.73 fm	2.73 fm
Binding energy**	128	128	128
BE (in MeV)			
BE/N (MeV)	8.0	8	8
Lorentz factor (γ)	4.51	64.41	214.71
E^{max} (MeV)	98.1	1392.3	4641.1
Duration time τ_d through Ag target component (sec)	$0.68 \cdot 10^{-18}$	$0.50 \cdot 10^{-19}$	$0.14 \cdot 10^{-21}$
References	Present work	[16, 22]	[7, 8]

Примечание. * [18], ** [19].

Table 5

The nuclear mean free paths and inelastic cross-sections compared with the corresponding ED mean free path and σ_{ED} for different projectiles at various energies

Type of projectile and energy	λ_{int} , cm	λ_{ED} , cm	σ_{int} , mb	σ_{ED} , mb	Reference
${}^7\text{Li}_3$ 3.0 A-GeV	15.2 ± 0.50	351.3 ± 49.6	1740.5 ± 20.0	50.50 ± 0.6	Present work
${}^{12}\text{C}_6$ 4.5 A-GeV	14.4 ± 0.33	236.0 ± 28.2	1837.2 ± 20.0	75.11 ± 0.5	Present work
${}^{16}\text{O}_8$ 4.5 A-GeV	12.18 ± 0.33	106.45 ± 10.68	2070.0 ± 140.0	91.2 ± 0.9	Present work
${}^{16}\text{O}_8$ 200 A-GeV	12.0 ± 0.20	96.0 ± 5.0	2620.0 ± 50.0	198.96 ± 11.3	[7]

binding energy per nucleon. The nucleus of ${}^7\text{Li}$ which contains seven nucleons, is smaller and has higher binding energy per nucleon than that of the ${}^6\text{Li}$ nucleus. Therefore the dissociation of ${}^6\text{Li}$ is easier than that of ${}^7\text{Li}$ in the case of interaction with the same target and at the same energy per nucleon. For this reason, the larger value of the ED events ratio for ${}^6\text{Li}$ than that for the ${}^{16}\text{O}$ nucleus at the same energy per nucleon could be anticipated. This is clear from the data given in Table 4.

2.3. Coulomb and Diffraction Dissociation Events

The fragmentation of the projectile can be induced by the strong nuclear interaction (specially at larger impact parameters) or by the electromagnetic field interaction. The basic idea [9] of Coulomb break-up is similar to that for electrodisintegration, but the cross-section is enhanced by Z_t^2 (where Z_t is the target charge number). The virtual photon method of Williams and Weizsacker [8–12] was used as a suitable way of considering the Coulomb effect in the fragmentation process. The Coulomb field of the target nucleus (in the projectile rest frame) appears as a packet of quasi-real photons of short time and enhanced by the Lorentz contraction factor

$$\gamma = (1 - v^2/c^2)^{-1/2}.$$

This collision time [1, 13] is roughly estimated by

$$t_d = b_{min}/\gamma c,$$

where b_{min} is the minimum impact parameter, equal to $R_p + R_t$. Consequently, the maximum photon frequency is contained in the electromagnetic field

$$\omega_{max} = c\gamma/b_{min}.$$

Also, this yields the maximum photon energy

$$E_\gamma^{max} = hc\gamma/(R_p + R_t).$$

According to this model, the electromagnetic pulse can be sufficiently energetic to excite giant resonance in the nucleus or to create lepton pairs or pions. From the basic assumptions of the model there is a flux of photons around the nucleus and the photon energy spectrum is compared classically [1, 11, 13–15] and treated by quantum mechanical calculations distinguished by the multiplicities of the photon spectrum. The values of γ and E_{γ}^{max} for an Ag target nucleus (the heaviest and most abundant element in the emulsion) for different projectiles and energies are estimated and listed in Table 4. It can be concluded that the values are 4.8, 4.8, and 3.2 for incident ^{16}O (4.5 A-GeV), ^{12}C (4.5 A-GeV) and ^7Li (3.0 A-GeV) respectively. The corresponding E_{γ}^{max} values are less than 100 MeV, which is smaller than the threshold energy for pionization, while for incident ^{16}O (60 A-GeV), it is equal to the value of producing pions having a mass about 140 MeV. But above the threshold for Δ -resonance (1232 MeV), for incident 200 A-GeV, it could produce Δ -resonance, which are subsequently dissociated into protons and pions. The present results for ^{12}C and ^{16}O strongly suggest that no pions are associated with the pure ED events. The pions accompanied the separated events due to diffraction dissociation is clear from Table 3 and confirm the present technique. It could be concluded that the technique of Ref. [23] can be used only at incident energy smaller than 10 A-GeV for light incident nuclei.

2.4. Mean Free Paths and Corresponding Cross-Sections

Table 4 represents the total observed inelastic, peripheral, and electromagnetic interactions. We can say that ED events as a percentage of the total number of events increase with the projectile energy. At the same time, the measured value of λ_{ED} decreases as the incident projectile charge and energy increase. The total inelastic cross-sections σ_{in} are estimated from the relation

$$\sigma_{in} = 1/n_{eff} \lambda_{in},$$

where n_{eff} in our type of emulsion is the effective density of emulsion nuclei

$$n_{eff} = \sum_i n_i \sigma_i / \sum_i \sigma_i = 3.78 \cdot 10^{22} \text{ atoms/cm}^3.$$

However, this number takes the value $3.2 \cdot 10^{22} \text{ atoms/cm}^3$ for the prepared emulsion in CERN SPS at 200 A-GeV [7, 14] where λ_{in} is taken as the observed mean free path for each beam. In order to obtain an absolute value for the electromagnetic dissociation cross-section σ_{ED} , the measured value of λ_{in} in the emulsion must be converted into an absolute cross-section on the Ag component, which is the heaviest and most abundant element in the emulsion. The estimated σ_{ED} for ED events on the Ag target is then calculated from the relation $\sigma_{ED} = f/\rho\lambda$, where $\rho = 1.028 \cdot 10^{22} \text{ atoms/cm}^3$ is the density of nuclei in the emulsion and $f = 0.67$ is a weight factor for this target component reaching unity for the emulsion as a whole.

The values of σ_{ED} as a function of the projectile charge are shown in Fig. 1b, for this work and other experiments [15]. This shows that σ_{ED} takes similar values despite the different detectors and reactions. It can be concluded that in spite of the heterogeneity of the emulsion target, it can be used generally to measure ED cross-section.

Figure 1a, b illustrates some experimental values of σ_{ED} as a function of projectile charge. The theoretical values of σ_{ED} calculated by the Weizsacker–Williams (WW) method [11] for relativistic heavy-ion reaction with ^{197}Au target at Bevalac energies [15] are also included. Here the calculated σ_{ED} values approach large values for both ultrarelativistic energy (100 A-GeV)

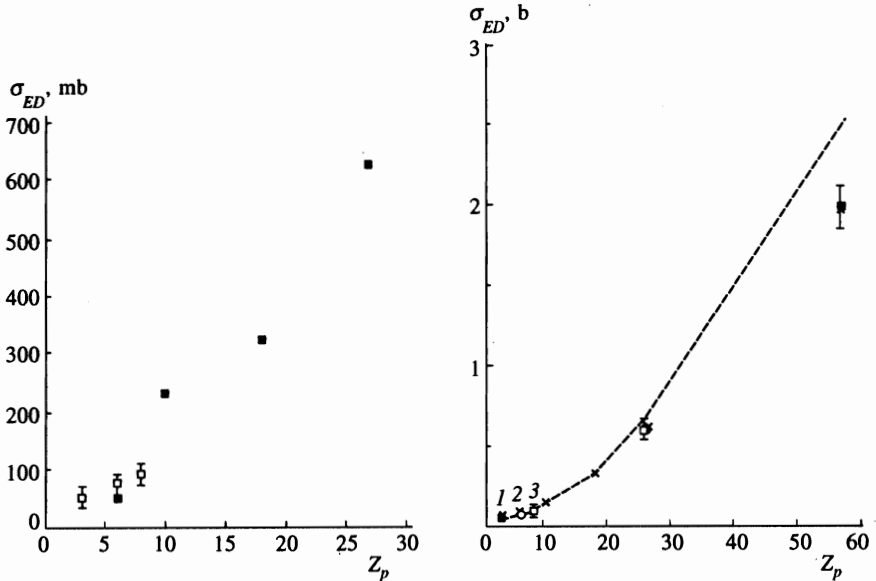


Fig. 1. *a* — The ED cross-section for the ${}^7\text{Li}$, ${}^{12}\text{C}$ and ${}^{16}\text{O}$ interactions at Dubna energy (3.0–4.5 A-GeV) as a function of projectile charge Z_p (■ — calculated, □ — experimental). *b* — Our experimental points ■ — 1, ○ — 2, □ — 3 for ${}^7\text{Li}$, ${}^{12}\text{C}$ and ${}^{16}\text{O}$ respectively at nearly the same energy. The points × represent the experimental values of σ_{ED} 's at different projectiles with ${}^{197}\text{Au}$ target. The corresponding calculated values according to WW-method are indicated by the dashed line

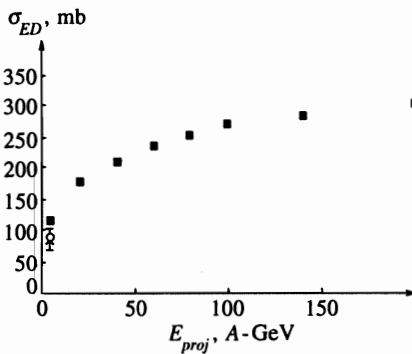


Fig. 2. The calculated ED cross-sections at different energies (■). The points ○ and × represent the experimental values of σ_{ED} 's for oxygen and carbon beams at 4.5 A-GeV

and high projectile charge, as noted in Ref. [15]. Also, the experimental and calculated values of the σ_{ED} cross-section for ${}^7\text{Li}$, ${}^{12}\text{C}$ and ${}^{16}\text{O}$ interactions as a function of projectile charge Z_p are shown in the same figure.

From this, it could be inferred that there is fair agreement between the present results for light projectile charge and calculated values at various energies.

The interactions of lithium, carbon and oxygen of the present work at Dubna energies are tabulated in Table 4. For comparison, the corresponding results of oxygen interactions at higher energies extracted from Refs. [7, 16, 17] are also included. As seen from Table 4 and Figs. 1 and 2, the percentage of ED events increases with both energy and incident beam charge.

Table 3 presents the different modes of carbon and oxygen breakup at 4.5 A-GeV inside the emulsion target (mainly due to the electromagnetic field of the Ag target nucleus component). Their numbers, fractions and observed partial cross-sections are listed. The majority of events lies in the channels producing 1He and 2He respectively. This reveals qualitatively that the relative production rates of α -particles in the projectile fragmentation processes are consistent with the values for different projectiles and energies [20]. The largest yield of ED events occurred in the case of emission of one He-fragment, associated with complete disintegration of the projectile. This result shows that with decreasing He multiplicity, the surface excitation energy of the projectile spectator increases. Also, the results confirm the same conclusions from the distributions of He fragments produced from nuclear events [21], which implies the limiting fragmentation behavior of the He-multiplicity distribution.

2.5. Dependence of the Electromagnetic Dissociation Cross-Section on Target Nucleus

Vidovic and Greiner et al. [31] have studied the impact-parameter dependence of electromagnetic particle production in ultrarelativistic heavy-ion collisions and directly deduced the equivalent photon method [11, 24] from quantum electrodynamics. It is well known that the simplicity of the photon method of Williams and Weizsacker [11] to be widely used [2, 7, 8, 15, 20–30] by scientists. A model [32] which depends on the WW-method [11] is proposed for the dissociation of relativistic nuclei in the Coulomb field of heavier nuclei which are easily excited or dissociated by a target nucleus.

In Ref. [33] the decay channels of ^{28}Si projectile dissociation to $p + ^{27}\text{Al}$, $n + ^{27}\text{Si}$ and $2p + ^{26}\text{Mg}$ using the WW-approximation with the experimental data for photonuclear cross-sections were examined, and it was found that there is no evidence for two-photon excitation of the ^{28}Si nucleus. In contract, the authors of Ref. [34] found large values for the neutron cross-section for electromagnetic dissociation of ^{197}Au targets by incident ^{20}Ne (1.7 A-GeV) and ^{86}K , ^{197}Au , ^{209}Bi beams with 1 A-GeV. They explained this observation by the dominant contribution from two-photon giant dipole excitation and interpreted the large cross-section as due to the Z_t dependence, since two-photon excitation will behave as Z_t^4 while one-photon excitation shows Z_t^2 behaviour (or $Z_t^{1.8}$ behaviour for heavy target nucleus), as found by the authors of Ref. [33].

3. CONCLUSIONS

The results confirm the dependence of the electromagnetic dissociation cross-section on both incident charge and energy. The measured ED cross-section has the same trend as the calculated one based on the Weizsacker-Williams method, and it increases with increasing of the projectile charge and energy.

For light projectiles, it was found that the largest yield of ED events occurred in the case of one He-fragment associated with complete disintegration of the projectile. This shows that with decreasing He fragment multiplicity, the surface excitation energy of the projectile spectator increases.

Calculations by the WW-method with data from counter experiments can be used to examine the decay channels for projectile dissociation by the excitation of the projectile nucleus, whereas other experiments interpret the ED of target nucleus in terms of the dominant contribution from two-photon giant dipole excitation.

Despite the heterogeneity of the emulsion target, it can be used to measure the ED cross-section.

The larger yield of ${}^6\text{Li}$ projectile dissociation than that for incident ${}^7\text{Li}$ may be due to the smaller binding energy per nucleon of the ${}^6\text{Li}$ nucleus.

References

1. R. Bhanja et al., Phys. Rev. Lett. **54**, 771 (1985).
2. C. A. Bertulani and G. Baur, Phys. Rep. **163**, 299 (1988).
3. H. H. Heckmen and D. E. Greiner, Phys. Rev. Lett. **28**, 926 (1972).
4. W. H. Barkas, *Nuclear Research Emulsions*, Academic, N. Y. (1963), Vol. 1.
5. E. J. Moniz et al., Phys. Rev. Lett. **26**, 445 (1971); M. N. Yasin, Ph. D. Thesis, Cairo University (1981).
6. H. H. Heckmen et al., Phys. Rev. C **17**, 1735 (1978).
7. G. Baroni et al., Nucl. Phys. A **516**, 673 (1990).
8. G. Baroni et al., Nucl. Phys. A **531**, 961 (1991); Preprint CERN-PPE/92-08 (1992); Preprint CERN-PPE/91-03 (1992).
9. X. Artru and G. B. Yodh, Phys. Lett. B **40**, 43 (1972).
10. T. D. Jackson, *Classical Electrodynamics*, Wiley, N. Y. (1962), p. 524; 2nd ed. (1975), p. 719.
11. C. F. Weizsacker, Z. Phys. **88**, 612 (1934); E. J. Williams, Phys. Rev. **45**, 729 (1934).
12. R. Jackle and H. Pilkuhn, Nucl. Phys. A **247**, 521 (1975).
13. G. Baur and C. Hoffman, Phys. Rev. C **30**, 247 (1984); C. A. Bertulani and G. Baur, Nucl. Phys. A **442**, 739 (1985); C. A. Bertulani and G. Baur, Nucl. Phys. A **458** (1986).
14. A. Goldberg, Nucl. Phys. A **440**, 636 (1984).
15. J. C. Hill et al., Phys. Rev. Lett. **60**, 999 (1988); Phys. Rev. C **38**, 1722 (1988); Phys. Rev. C **39**, 524 (1989).
16. G. Sing and P. L. Jain, Intern. Rept. Aug. **29** (1991).
17. M. El-Nadi et al., Egypt. J. Phys. No. 1-2 (1993).
18. C. Douglas and A. Giancoli, Physics (Principles with Application), 3rd ed. Prentice-Hall Int. Ed. (1991). In this book, the data are taken from Brookhaven Nat. Lab. (1990).
19. E. G. Fuller., Phys. Rep. **127**, 3 (1985); C. W. DeJager et al., Atomic Data and Nucl. Data Tables **14**, 479 (1974).
20. M. I. Adamovich et al., Phys. Rev. C **40**, 66 (1989), Preprint EI-10838, JINR, Dubna (1977).
21. D. L. Olsen et al., Phys. Rev. C **24**, 1529 (1981); H. M. Heckmen et al., Phys. Rev. **37**, 56 (1976).
22. G. Sing and P. L. Jain, Phys. Rev. C **41**, 999 (1990).
23. M. Nabil Yasin, J. Fac. Educ. Ain Shams Univ., № 19, 145 (1994); Preprint ICTP Rep. IC/194/389, Trieste, Italy.
24. E. J. Williams, Proc. R. Soc (London) A **139**, 163 (1933); E. Fermi, Z. Phys. **29**, 315 (1924).
25. G. Baur and L. G. Ferreira, Nucl. Phys. A **518**, 786 (1990).
26. B. Muller and A. J. Schramm, Phys. Rev. D **42**, 3699 (1990).
27. E. Papagerorgiu, Phys. Lett. B **250**, 155 (1990); M. Drees, J. Ellis, and D. Zeppenfeld, Phys. Lett. B **223**, 454 (1989).
28. R. N. Cahn and J. D. Jackson, Phys. Rev. D **42**, 3690 (1990).
29. K. J. Abraham et al., Phys. Lett. B **251**, 186 (1990); C. Hofmann et al., Phys. Lett. B **262**, 210 (1991).
30. J. Eicher, Phys. Rept. **193**, 165 (1990).
31. M. Vidovic, M. Greiner, C. Best, and G. Soff., Phys. Rev. C **47**, 2308 (1993).
32. H. Pilkuhn, Phys. Lett. B **38**, 143 (1972).
33. J. Sonnadara Upul, Nucl. Phys. A **569**, 149 (1994).
34. T. Aumann et al., Nucl. Phys. A **569**, 157 (1994).